JOURNAL OF PROPULSION AND POWER
Vol. 14, No. 5, September–October 1998

Cycles for Earth-to-Orbit Propulsion

Detlef Manski,* Christoph Goertz,† and Hagen-D. Saßnick‡
DLR, German Aerospace Center, Lampoldshausen D-74239, Germany
James R. Hulka§
Aerojet, Sacramento, California 95813
and
B. David Goracke¶ and Daniel J. H. Levack**
The Boeing Company, Canoga Park, California 91309

The reduction of Earth-to-orbit launch costs in conjunction with an increase in launcher reliability and operational efficiency are the key demands on future space transportation systems. Results of various system analyses indicate that these demands can be met with future single-stage-to-orbit (SSTO) vehicles using advanced technologies for both structure and propulsion systems. This paper will provide a classification and description of all turbopump feed liquid rocket engine cycles, followed by a combined vehicle/propulsion analysis of the design parameters for the propulsion systems and their associated thermodynamic cycles for the launch of future SSTO vehicles. Existing and projected rocket engine cycles capable of SSTO missions will be presented.

I. Introduction

LAUNCHERS that are able to deliver a payload into low Earth orbit using only a single-stage rocket require advanced technology for both the vehicle and the propulsion system and, in addition, high-performance rocket engine cycles. The emphasis in this paper is on the analysis of the design parameters of the propulsion cycles that make single-stage-to-orbit (SSTO) feasible. On the one hand, thermodynamic cycles with higher combustion chamber pressures increase the performance of the liquid rocket engines for SSTO vehicles; on the other hand, this chamber pressure increase is often linked with an increase in engine system weight that reduces the gain in performance. The tradeoff between performance and vehicle mass will be shown. Definitions, notations, and terms follow standard usage.[1]

II. Scope

Two categories of thermodynamic cycles could be used to feed the propellants from the low-pressure tanks to the high-pressure main combustion chamber: The pressure feed cycle or the turbopump feed cycle. Because high chamber pressure will be necessary for SSTO propulsion systems, pressure feed cycles are not applicable to the launch of SSTO vehicles because of the excessively high tank pressures required. The pressure feed cycle is foreseen for use in small upper-stage propulsion systems, for trajectory and attitude-control propulsion systems, and to provide prepressurization of the launchers' main tanks, which require a certain pressure for stability and initial turbopump suction pressure, taking into account hydrostatic pressure from the flight. Pressure feed cycles could be classified as pressurant tank, gas-generator plenum, hypergolic injection, blowdown and superblowdown systems. More detailed information about pressure feed cycles and the optimization of small spacecraft propulsion systems is available elsewhere.[2,3]

Consequently, this paper concentrates on turbopump feed propulsion cycles, which generate internally the high pressures required for SSTO vehicles. A classification of turbopump liquid rocket engine cycles is shown in Table 1 for single-mode cycles and in Table 2 for dual-mode cycles. A single-mode cycle operates more or less at one state point with fixed geometry hardware, having no means to substantially change specific impulse. A dual-mode cycle has two operating state points, with changes caused by the use of separate engines, different propellants or mixture ratios, or geometry variations brought about mechanically or thermodynamically.

III. Candidate Descriptions

A. Staged Combustion Cycles

The staged combustion cycle has the highest performance of all single-mode rocket engine cycles. The expansion of all propellants from a high chamber pressure makes it possible to attain high specific impulse. However, there is a limit in chamber pressure for the staged combustion cycle because of the limited energy available to drive the turbines. This pressure depends on specific features of the staged combustion cycle type, allowable temperature in the turbines, turbine and pump efficiencies, and pressure ratios in the cooling system and injectors. Accessible chamber pressure as a function of these parameters is plotted in Manski and Martin.[4]

Four subcategories of the staged combustion cycle are shown in Figs. 1–4. Staged combustion cycles with fuel- and oxidizer-rich preburners and with split pumps are shown in Figs. 1 and 2. The full-flow staged combustion cycle with complete preburning, oxidizer and fuel rich, is shown in Fig. 3. A more complex full-flow staged combustion cycle with an additional pump for power matching between the oxidizer and fuel, which will keep preburner entry pressures on the same level, is shown in Fig. 4. The additional pump is clutched on the fuel turbopump shaft but driven by a partial oxidizer mass flow. Whether this additional pump must be clutched on the oxidizer turbopump shaft and driven by a partial fuel mass

Received Sept. 2, 1997; revision received April 29, 1998; accepted for publication May 21, 1998.

*Head, System Analysis, Space Propulsion, Dr.-Ing. E-mail: detlef.manski@dlr.de. Member AIAA.
†Aerospace Engineer, Space Propulsion.
‡Aerospace Engineer, Space Propulsion, Dr.-Ing.
§Engineering Specialist, Aerojet Propulsion Division, P.O. Box 13222. E-mail: hulka_james@aphub.aerojetpd.com. Senior Member AIAA.
¶Director, Rocketdyne Division, Advanced Concepts and Technology. Member AIAA.
**Program Manager, Rocketdyne Division, System Analysis.

Table 1 Single mode cycles

Integral flow (main flow, closed) cycle	Staged combustion cycle	Fuel-rich preburning	Fig. 3, Ref. 4
		Fuel-rich preburning with split oxygen pump	Fig. 1
		Oxidizer-rich preburning	Fig. 7, Ref. 4
		Oxidizer-rich preburning with split hydrogen pump	Fig. 2
		Complete preburning fuel- and oxidizer-rich (full-flow)	Fig. 3
		Fuel- and oxidizer-rich preburning and auxiliary pump for pressure balance	Fig. 4
	Expander, topping cycle	Expander simple	Fig. 10
		Split expander	Fig. 11
		Expander with internal heat exchanger	Fig. 12
	Mixed expander staged combustion cycle	Boost pump expander	Fig. 28
		Hybrid ox-side expander	Fig. 13
		Invers hybrid fu-side expander	Fig. 14
Derived flow (secondary flow, bypass, open) cycle	Gas-generator cycle	Oxidizer-rich gas-generator	
		Fuel-rich gas-generator	Fig. 5
		Fuel- and ox-rich gas-generator	
	Tap-off cycle		Fig. 6
	Expander bleed cycle	Expander bleed simple	Fig. 7
		Expander bleed split flow	Fig. 8
	Mixed expander/gas-generator cycle		
Mixed derived and integral flow	Expander bleed and topping cycle		Fig. 9
	Dual thrust chamber (afterburning in the derived stream)		Fig. 15
	Gas-generator topping staged combustion cycle		Fig. 19

Table 2 Dual mode cycles

Single fuel	Dual mixture ratio	
	Dual position nozzle	Fig. 11, Ref. 13, pp. 1.7–11
	Dual shape (bell) nozzle with controlled flow separation	Fig. 7, Ref. 13, pp. 1.7–7
	Dual engines	
	Dual cycles (staged combustion/gas-generator combined cluster)	Fig. 18, $fu_1 = fu_2$
	Dual throat, dual expander	Fig. 16
Dual fuel (tripropellant cycles)	Dual engines	
	Dual cycle (staged combustion/gas-generator combined cluster)	Fig. 18
	Dual throat, dual expander	Fig. 16
	Dual fuel combustion chamber	Fig. 17

flow or reverse, as in Fig. 4, depends on propellant combination, main combustion chamber mixture ratio, chamber pressure, and preburner mixture ratios.

B. Gas-Generator Cycles

Gas-generator cycles can be classified into three main categories: 1) fuel-rich, 2) oxidizer-rich, and 3) dual gas-generator type, having both oxidizer- and fuel-rich gas-generators. The defining characteristic of the gas-generator cycle is that the secondary exhaust flow that drives the turbopump system is not expanded from the high-pressure chambers. Because of low temperature and pressure at the exit of this derived flow, the average specific impulse of this cycle is lower than for staged combustion cycles. In addition, tank masses and structures are increased because of a different mixture ratio in the main tank and engine, particularly for hydrogen-rich gas-generators.

As an example of a secondary flow cycle, the fuel-rich gas-generator cycle is shown in Fig. 5. Because of the large mass of oxygen required to drive the turbine, an oxidizer-rich (ox-rich) gas-generator cycle is not practical.

C. Tap-Off Cycle

A gas generator can also be implemented by using a tap-off cycle. In this cycle, fuel-rich combusted gases are extracted (tapped-off) from the periphery of the main combustion chamber, where mixture ratios are kept low to help cool the chamber wall, and then routed to the turbines (Fig. 6). The physical gas-generator is replaced by the main combustion chamber. One example of the tap-off cycle engine is the J-2S, a redesign of the fuel-rich gas-generator cycle J-2 engine used in the Saturn vehicles. In a nozzle tap-off cycle described by Kozlov et al.,[5] turbine drive gas is taken from the boundary layer of the supersonic nozzle and reinjected at a downstream location.

D. Expander Cycles

In the cycles described in the previous text, the turbines are driven by hot gases generated by gas-generators, preburners, or even main combustion chambers. Expander cycles use heat from the regenerative cooling system or even from heat exchangers in the main combustion chamber. Because these heat transfers are of limited energy, the chamber pressures that

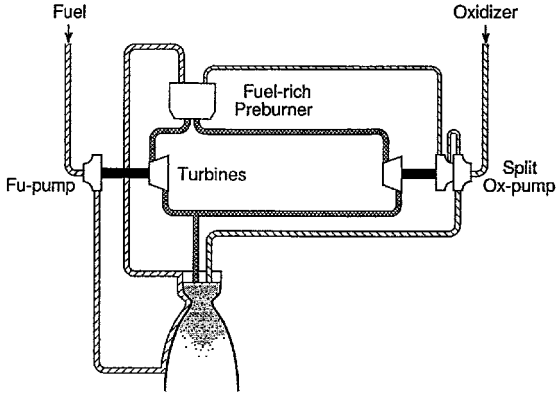

Fig. 1 Staged combustion cycle with fuel-rich preburners and split oxidizer pump.

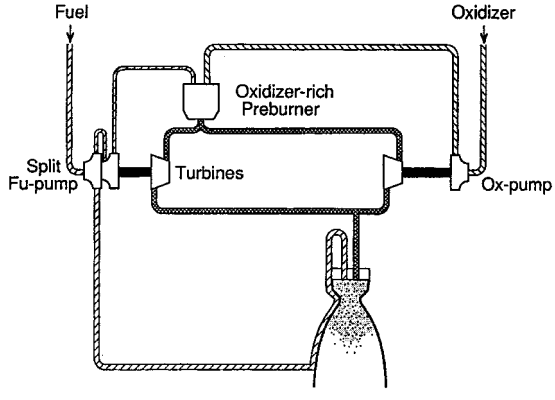

Fig. 2 Staged combustion cycle with oxidizer-rich preburners and split fuel pump.

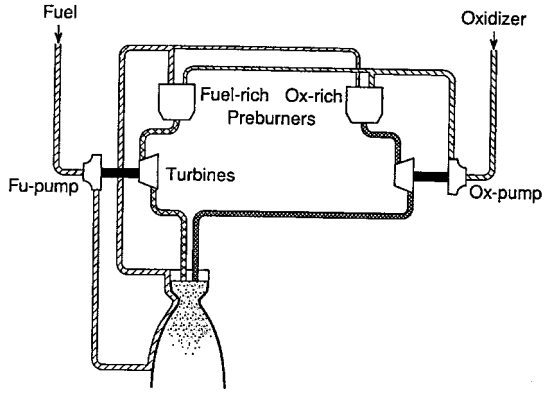

Fig. 3 Simple full-flow staged combustion cycle with oxidizer- and fuel-rich preburners.

could be reached by these cycles are lower than those reached by gas-generator or staged combustion cycles. However, the main advantages of the expander cycle are simplicity, a lightweight turbopump system, and a smooth ignition and startup sequence because of the absence of any gas-generator or preburner. The low engine weight that could be realized with this cycle compensates for the disadvantage of the relatively low chamber pressure. Studies of these cycles are discussed in Refs. 6 and 7.

Figure 7 shows the basic form of a simple expander bleed cycle. The turbopump of this cycle has a split pump to compensate for different pressure losses in the cooling flows of the nozzle and chamber. The coolant flow then drives two turbines in parallel, before it is injected into the nozzle skirt. Figure 8 shows the expander bleed cycle with a split pump for the combustion chamber cooling flow. Nozzle cooling is supplied by

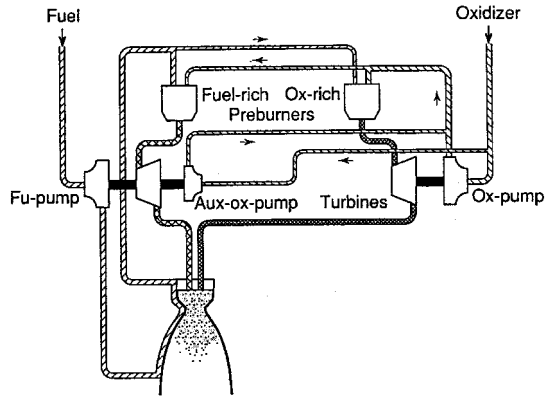

Fig. 4 Full-flow staged combustion cycle with oxidizer- and fuel-rich preburners and an auxiliary pump for matching preburner entry pressure.

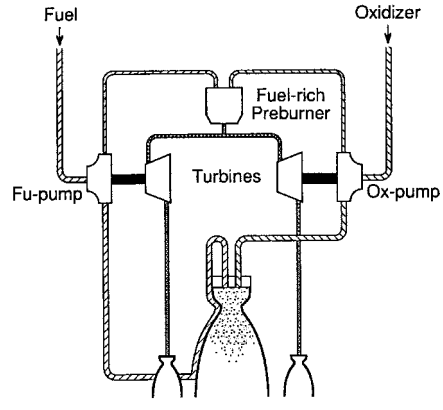

Fig. 5 Fuel-rich gas-generator cycle.

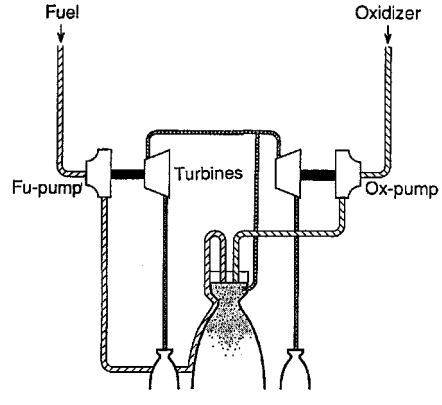

Fig. 6 Fuel-rich tap-off cycle.

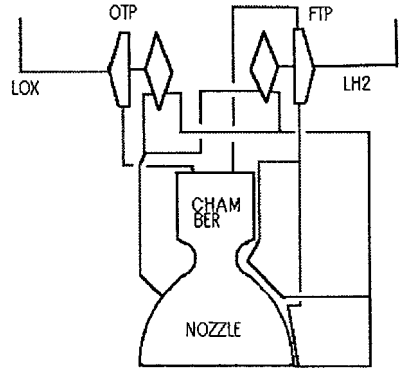

Fig. 7 Simple expander bleed cycle.

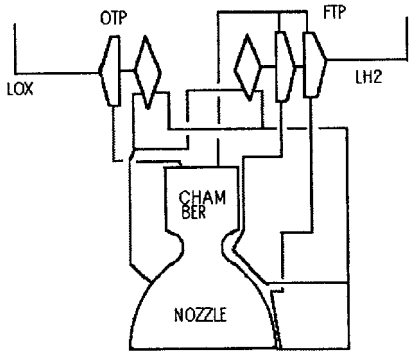

Fig. 8 Expander bleed cycle with split pump and cooling flow.

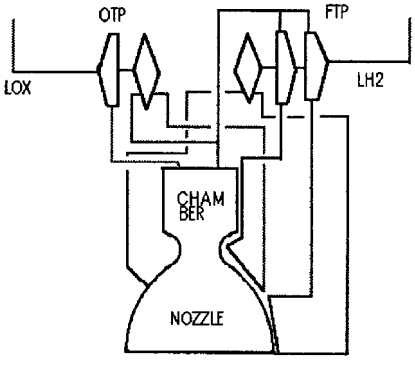

Fig. 9 Expander split cycle fuel-bleed and oxidizer topping.

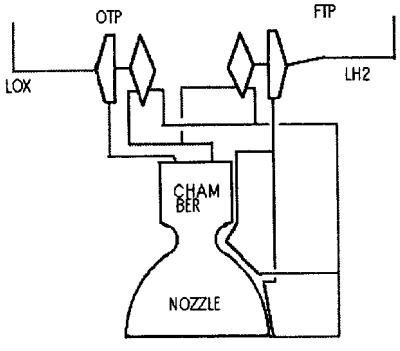

Fig. 10 Expander topping cycle.

the flow from the main pump, which reduces the mass of and stress on the nozzle extension. Figure 9 shows an expander split cycle bleed and topping, with derived flow for the fuel turbine and integrated flow for the oxidizer turbine. After expansion in the oxidizer turbine, the main chamber cooling flow from the split fuel pump is directly introduced into the main chamber, as is usual in integrated flow cycles. After nozzle extension cooling and expansion into the fuel turbine, the second flow is introduced into the nozzle skirt, as normally done in derived flow cycles.

Figure 10 shows an expander topping cycle. All of the fuel is used for cooling and is then injected into the main chamber after expansion in both turbines. Therefore, the exit pressure of both turbines must be higher than the chamber pressure. Figure 11 shows a split expander topping cycle. Only the split pump supplies cooling flow to the chamber and nozzle. The heated fuel from the cooling channels drives the turbines and is added to the fuel from the main pump before being injected into the combustion chamber.

Because the turbine drive gas has less energy, the chamber pressures of expander cycle engines are lower but can be increased by special design features of the engine, such as a long combustion chamber, smaller engines, or high-aspect-ratio cooling channel designs.[6] Even higher chamber pressures

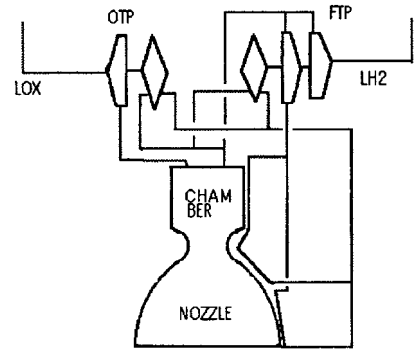

Fig. 11 Expander split topping cycle.

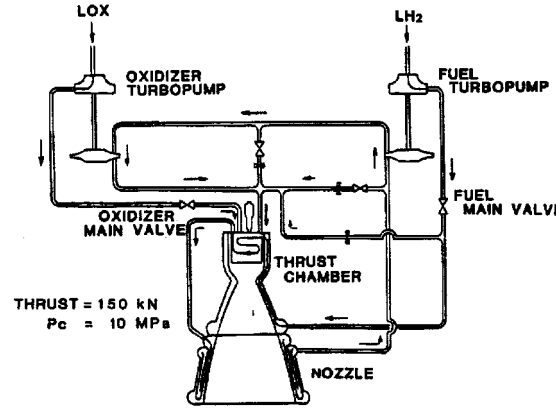

Fig. 12 Expander cycle using internal heat exchanger in the combustion chamber.

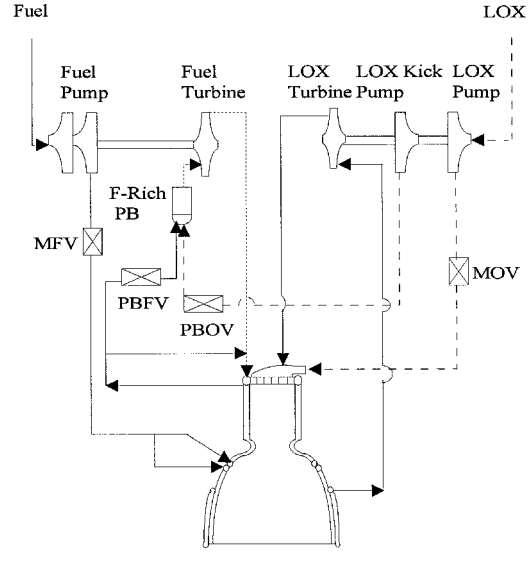

Fig. 13 Hybrid cycle: fuel-side preburner, oxidizer-side expander.

could be reached using an additional heat exchanger in the combustion chamber. Figure 12 shows an expander cycle with a heat exchanger inside the combustion chamber as proposed by Tanatsugu et al.[8]

A mixed expander/staged combustion cycle, the hybrid cycle, is shown in Fig. 13 and described in more detail by Goracke et al.[9] This closed cycle uses a hydrogen preburner to power the fuel pump, because the fuel pump needs more power than the oxygen pump, and a fuel expander to power the oxygen pump. The inverse of the hybrid cycle, shown in Fig. 14, has a preburner powering the oxygen pump and a fuel expander powering the fuel pump.

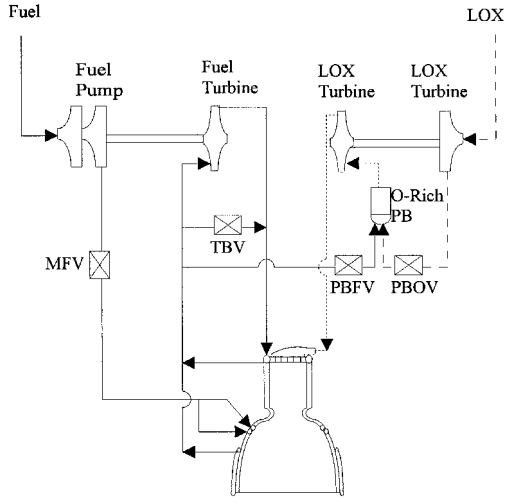

Fig. 14 Inverse hybrid cycle: oxidizer-side preburner, fuel-side expander.

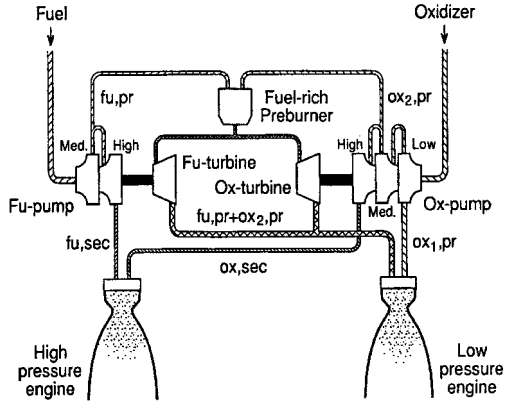

Fig. 15 Dual-thrust chamber cycle, afterburning in gas-generator stream.

E. Dual-Thrust Chamber Cycle

The low performance of the gas-generator cycle could be augmented by afterburning the gas-generator stream to increase the specific impulse of that branch. Figure 15 shows this dual-thrust chamber cycle, which could also be termed gas-generator cycle with afterburning in the secondary stream, or dual-bell cycle.[10] This cycle has a dual-split fuel pump and a triple-split oxidizer pump. The disadvantage of the gas-generator cycle, increased net mass, is reduced. The two branches of the dual-bell cycle could be interpreted as a staged combustion branch and a gas-generator branch. Therefore, this cycle has the advantages of both the staged combustion cycle, with its high performance, and the gas-generator cycle, with modest pressure requirements in the turbopump system. This cycle does not, however, necessarily result in a net advantage. It also has lower performance than the pure staged combustion cycle. An additional advantage, which is not necessarily unique to this cycle, is that the two thrust chambers have a common turbopump system, which results in lower specific mass. An important characteristic of the dual-thrust chamber cycle is that it operates at lower preburner pressures than the staged combustion cycle. Because of the afterburning of the fuel-rich gas-generator stream, the secondary thrust chamber could be designed for a higher chamber pressure and higher mixture ratio than the normal secondary flow of the gas-generator cycle.

F. Dual-Expander Cycle

The dual-expander cycle proposed by Beichel[11] is shown in Fig. 16. The dual-expander engine consists of two combustion chambers, the primary outer chamber and secondary inner

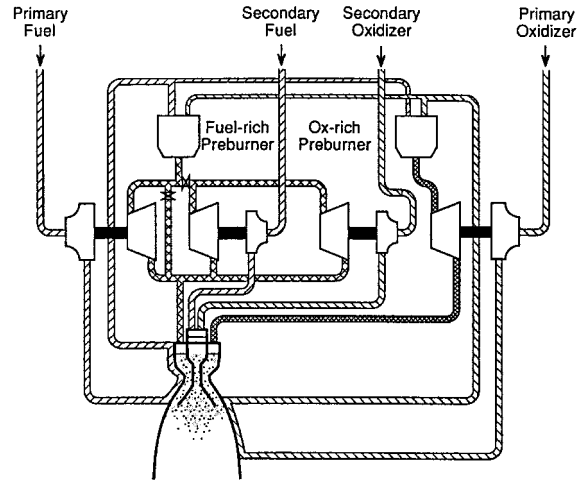

Fig. 16 Dual-expander cycle.

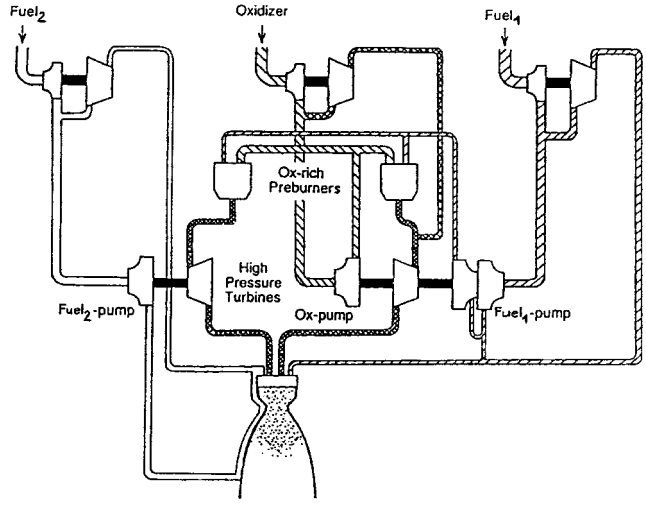

Fig. 17 Tripropellant cycle.

chamber; four turbopumps, two ox-turbopumps and two fuel-turbopumps; and fuel-rich and ox-rich preburners. In the primary chamber H_2/O_2 is burned, and in the secondary chamber dense fuels such as propane, methane, or kerosene, or even hydrogen at a higher and therefore more dense mixture ratio, are burned. At liftoff, both chambers are operated in parallel (mode 1). After burnout of the secondary propellant, mode 1 is completed and the secondary chamber is cut off. The primary chamber continues to burn using the primary and the secondary exit area, so that the specific impulse for mode 2 is higher.

Important design parameters for this kind of dual-mode propulsion are the thrust split, the ratio of primary chamber thrust to the total thrust at sea level, the propellant mass ratio, and the ratio of propellant mass consumed by the primary chamber to the total propellant mass. Parametric studies of the dependencies among these parameters are available.[4,10,12]

The dual-expander and the dual-throat cycle are only slightly different from each other. The dual-throat has two combustors with throats in series, whereas the dual-expander has two combusters with throats in parallel. Engine cooling and nozzle performance differ between the two, as do their technology requirements.

G. Dual-Fuel Combustion Chamber Cycle

The dual-fuel combustion chamber or tripropellant cycle with an ox-rich preburner is shown in Fig. 17. It has three high-pressure pumps, for hydrogen, oxygen, and kerosene. The kerosene system has a split pump, which provides the fuel for

the two ox-rich preburners. The kerosene and oxygen pump are driven by a common turbine and the hydrogen by a second turbine. The additional three boost pumps are used for prepressurization of the propellant, and they are driven by separate turbines. The two fuel turbines are driven hydraulically by high-pressure fuels and the oxygen boost turbine is driven by preburned ox-rich propellant, which is then introduced into the oxygen.

H. Dual-Mixed Cycles

The staged-combustion/gas-generator combined cluster is shown in Fig. 18. A staged-combustion/gas-generator combined cluster consists of two combustion chambers with common turbopump feed systems. One part is an H_2/O_2 staged combustion engine, the other part has a hydrocarbon/oxygen combustion chamber, and the turbopumps are driven by H_2/O_2 gas from the H_2/O_2 preburner, which is then dumped, so that this part of the system has essentially a gas-generator cycle. At liftoff, both engines are operated (mode 1). After burnout of the hydrocarbon propellant, only the H_2/O_2 engine is operated (mode 2).

The gas-generator combined cycle on top of a staged combustion cycle is shown in Fig. 19. This cycle begins with preburning at relatively low pressure to deliver the work necessary for the initial low-pressure pumps. The preburned exhaust gases are expanded first in the low-pressure turbines and then in the auxiliary nozzles. This represents the gas-generator-derived flow cycle. The initially low-pressure main propellants

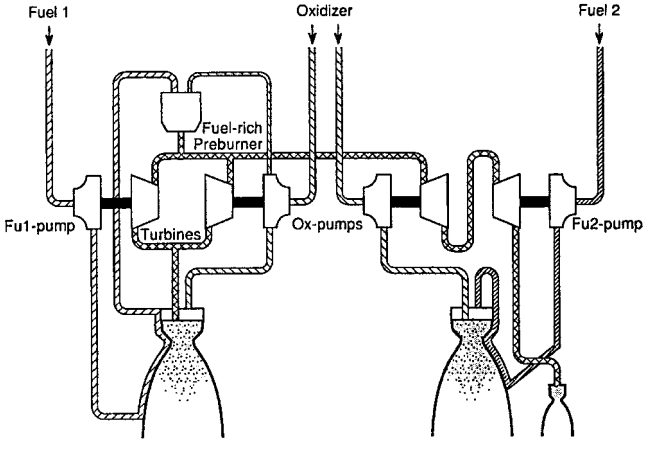

Fig. 18 Staged combustion/gas generator combined cluster.

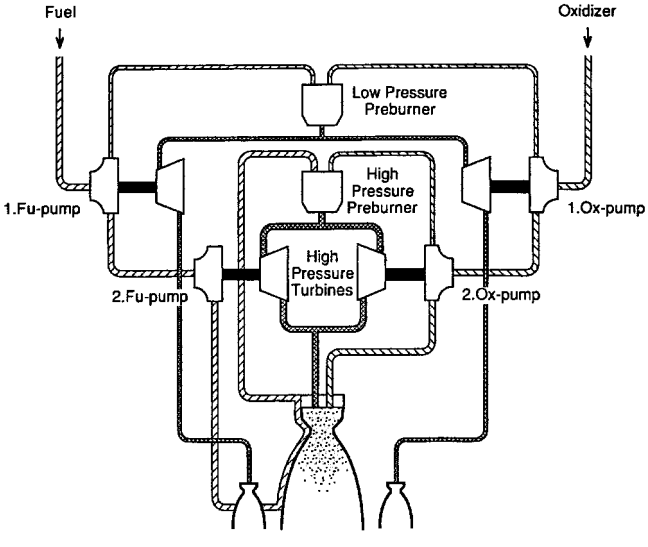

Fig. 19 Combined cycle gas-generator topping staged combustion.

are pumped to higher pressures again by the staged combustion cycle. This combined cycle allows higher chamber pressure than the normal staged combustion cycle. However, the advantages of the higher-pressure capability may be eliminated by the increased net mass necessary for the additional subsystems.

I. Dual Engine Cycle

The use of two different engines, one of which is switched off during ascent of the rocket, is defined as a dual-engine propulsion cycle. The first type of engine could be chosen to meet lower atmosphere flight requirements, that is, dense propellants, such as hydrocarbons or high-mixture-ratio hydrogen, and shorter nozzles, so that the specific impulse is better adapted to that altitude. The second could be designed for less dense propellants and longer nozzles, to have optimum propulsion parameters for the second flight phase.

J. Dual-Mixture Cycle

A dual-mixture-ratio propulsion cycle is defined as using different mixture ratios during the ascent of a rocket. This propulsion cycle could be effectively used with H_2/O_2 propellants, which have the most significant density differences for low- and high-mixture ratios. The high, and therefore more dense, mixture ratio with low specific impulse is used during boost as mode 1, and the lower mixture ratio with higher specific impulse is applied at end of the trajectory. The time of the switch to mode 2 must be optimized. To achieve the lower mixture ratio, the oxygen mass flow can be reduced while keeping the hydrogen mass flow constant. This approach provides a reduction in chamber pressure for the lower mixture ratio. The lower chamber pressure has almost no effect on specific impulse because the pressure ratio remains constant and the atmospheric pressure is drastically reduced before mode change.

K. Dual-Nozzle Extension

This dual-mode propulsion system contains a two-position extendible nozzle for adaption to decreasing ambient pressure during rocket ascent. Hagemann et al.[13] show a sketch of the two position nozzle (Fig. 11) and describe this propulsion cycle concept.

L. Dual-Bell Nozzle

Hagemann et al. also show a sketch of the dual-bell nozzle (Fig. 7). The dual-bell, or dual-shape, nozzle permits effective operation at sea level and under vacuum conditions. The nozzle from the throat to a moderate expansion ratio is contoured for sea-level operation. At that point the nozzle has a step change in its contour to blend to a new shape for altitude operation. The nozzle is compatible with nearly all engine cycles and will improve the mission-average specific impulse for SSTO engines over single-bell nozzles. Some performance loss is encountered because of nonoptimum shaping and shocks generated at the shape transition point. Other issues of concern with this nozzle approach are its increased length and weight and the control of the flow transition from small to large contours.

M. Aerospike and Plug Nozzles

The aerospike nozzle expands combustion exhaust gases against a central converging spike to produce thrust, and uses ambient pressure to define the outer flowfield boundary; in concept, it is a bell engine turned ''inside out,'' and compensating for altitude effects. The aerospike nozzle is usually truncated, so that it is one-third the length of a bell nozzle. The aerospike also has vehicle-integration advantages, because it can be sized easily to fill a vehicle's base area, and the thrust is taken out efficiently at the periphery of the engine to the vehicle skin structure.

In contrast to a conventional bell engine, combustion in an aerospike thrust chamber assembly occurs in an annulus along

the outer edge of the nozzle. This fact has several important consequences: The throat dimensions are small because the combustion flow has to be spread over a larger dimension, the fluids have to be routed further to be combusted, and the throat heat flux is higher. As a result, multiple low-expansion combustors are required to better control throat dimensions, heat transfer, and flows. While the aerospike nozzle is compatible with all of the engine cycles discussed in this section, it is best suited to the gas-generator cycle for several reasons:

1) The altitude performance compensation feature neutralizes the lower chamber pressure.

2) The extended feed system ducting penalizes cycles that require large (in terms of weight) gas flow ducting.

3) The gas-generator exhaust bleed through the base of the truncated spike improves its otherwise poor nozzle efficiency by reducing base drag.

The aerospike has several configuration alternatives. Ordinarily, the central spike is truncated for engine weight and dimension reasons. The nozzle can be configured in a round, axisymmetric geometry, so that the combustors lie around a circle, or it can be configured as a linear aerospike, so that the combustors lie in a line and exhaust over a planar geometry. The round aerospike can be distorted into ellipses or other shapes to fit a vehicle base, and the linear aerospike can be one- or two-sided (two one-sided nozzles back-to-back).

IV. Cycle Modeling

A. Combined Vehicle/Propulsion Analysis

Over the past several years, the propulsion system analysis method launcher system Analysis (ST) has been developed and applied to compare and analyze various kinds of rocket engine cycles for the future space transportation systems. The rocket launcher analysis tool ST[4,12,14–17] uses physically related equations for each subsystem and thermodynamic methods for the performance data. The models used in the tool consist of engine performance calculations, simplified engine cycle calculations, engine mass calculations, vehicle mass calculations, vehicle performance calculations, and trajectory calculations. This program allows analysis of the rocket engine and vehicle interaction with the capability to evaluate the effects on vehicle design of numerous parameters such as payload mass, engine type, propellant combination, and nozzle exit pressure. The thermodynamic cycles and their subcycles that were actually included in the ST space propulsion system analysis are listed elsewhere.[18] Two-dimensional performance analysis tools[19–22] can be linked to ST. ST was used for the comparative cycle analysis in this paper.

B. Cycle Analysis

During the last few years, the SEQNEW[23] method has been developed for the analysis of complex liquid rocket engine cycles. The basic idea for the method was taken from similar cycle analyses of complex powerplant processes with a large number of different components. A modular approach has been chosen for this analysis, i.e., an engine cycle is assembled from elements of a predefined component library (pumps, turbines, gas-generator, combustion chamber, nozzle, valves, etc.), and a sequential method employed. The components of an engine cycle are calculated repeatedly in a predetermined sequence until the desired solution state is achieved. There are several advantages of the sequential method. First, the modeling of components in separate subroutines makes possible a wide range of modeling from simple to sophisticated, depending on the accuracy required. Existing subroutines can be integrated easily, and new component models can be developed independently and integrated when needed. Second, the sequential method is a rather intuitive approach, which is quickly understood by the engineer. Complex engine cycles can be assembled gradually, which allows for checks and early detection of coding errors.

C. Transient Cycle Analysis

For a complete understanding of a liquid rocket engine cycle the transient behavior is as essential as the stationary performance. The quality of a startup sequence depends on characteristics of pumps, turbines, and lines, and is influenced to a large extent by valve sequences. The mathematical model BEGDYN[24] was developed to simulate the transient behavior of cryogenic rocket engine cycles. As an example of the capabilities of BEGDYN, the startup transient of the gas-generator cycle engine Vulcan was simulated.[25]

V. Cycle Comparisons

A. Reference Vehicle

For this comparative cycle analysis the chosen reference vehicle was the same as that used in Manski and Fina,[15] an SSTO vertical-take-off and landing vehicle, because this vehicle is most sensitive to propulsion parameter variations. The vehicle is of the BETA- or Delta Clipper type, following a re-examination by Manski and Fina. The original vehicles are defined by Koelle and Kleinau[26] and Weegar.[27] These vehicles have a great need for potential future technology. The vehicles are presented in Manski and Fina in figures along with a mass breakdown comparison with ST simulation.

The number of engines integrated in this SSTO launcher was assumed to be eight, except for some dual-mode cycles such as the dual-expander or dual-thrust chamber, where the number of engines was four, because these dual-mode engines have a duplication of components such as nozzles, chambers, and turbopumps. The neccessary thrust reduction at maximum allowable acceleration could be realized by reducing chamber pressure or by switching off two engines located opposite to each other. The trajectory analysis was performed by POST.[28] The switchoff sequence was not input, and in that chamber pressure reduction was assumed to keep the acceleration at the allowable $3g_0$ maximum. This results in a small advantage for the single-mode cycles, because the dual-mode engines have a built-in acceleration reduction capability, achieved by shutting down the secondary flow. The total engine thrust in mode 2 is then provided only by the primary flow. The time of shutdown of the secondary flow is determined by the stage parameter mass split ratio m_r. The thrust split ratio is F_r. The characteristics for the vehicle model and propulsion model that were assumed are shown next. Vehicle model: ST-vehicle mass model[16]; landing gears, propellants tanks for re-entry[15]; eight engine single-mode, 4 + 4 engine for dual mode, four engine for dual expander and dual-bell; three (tripropellant) or two cylindrical tanks, eliptical 2/3 end caps, tank diameter of 8 m, no common bulkheads, minimum tank wall thickness 6 mm; constant payload of 16.5 mg and payload fairing of 2.6 mg into a 200-km circular orbit from French Guyana, Kourou, following trajectory optimization[29]; acceleration limit $3g_0$; takeoff acceleration $1.4g_0$ as optimized[29]; and dual-mode mass split ratio $m_r = m_{8_{\text{pri}}}/(m_{8_{\text{pri}}} + m_{8_{\text{sec}}})$. Propulsion model: ST-performance, cycle, and engine mass model[4,16]; preburner mixture ratios: fuel-rich 0.85:1 for hydrogen, ox-rich 100:1 for hydrogen, 42:1 for propane, 40:1 for methane; efficiencies for all turbines and pumps at 75%; pressure-loss ratios in cooling tubes, lines and injectors are assumed to be independent from chamber pressure and constant, taken from the SSME cycle; pressurants = helium for oxygen, hydrogen for hydrogen and for hydrocarbon in dual-mode, He for hydrocarbon in single-mode; He pressurant temperature = 100 K for hydrocarbon in single-mode, 20 K for hydrogen and dual-fuel; nozzle exit pressure 0.3 bar, dual expander 0.35 bar as optimized[29]; constant η_{c^*} and η_{c_F} efficiencies of 99 and 98%; and dual-mode thrust ratio $F_r = F_{\text{pri}}/(F_{\text{pri}} + F_{\text{sec}})$.

The third assumption for the propulsion model leads to small advantages for all open cycles. Low-pressure ratio, full-flow, closed-cycle turbine efficiencies are significantly higher than high-pressure ratio, low flow rate, open-cycle ones. These ef-

ficiencies have a direct influence on open-cycle engine performance and an indirect influence on closed-cycle engines. Because the gas-generator cycle has lower performance in SSTO vehicles, this assumption may be sufficient in the following analysis.

B. Cycle Optimization

The optimizations were made for a constant payload into a circular low Earth orbit and return of the single-stage launcher to Earth by minimizing the effective net mass of the SSTO vehicle (dry mass plus reserve and residual propellants). A low effective net mass is one of the criteria for a minimal-cost launcher system. The comparisons were made vs the design propulsion parameters, chamber pressure, mixture ratio, propellant combinations of hydrocarbons, and hydrogen with oxygen for the given constant parameters. In the case of dual-mode cycles, a multiplication by their primary and secondary parameters occurs, along with two new parameters, propellant split and thrust split ratio, which increase the variations.

C. Single-Mode Cycles

1. Staged Combustion Cycle

The highest performance with any single-mode cycle is obtained by the staged combustion cycle using H_2/O_2 as propellant with only one fuel-rich preburner and split pump (Fig. 1). The performance of this cycle is plotted in Fig. 20 for various mixture ratios and chamber pressures. Lowest effective net mass of the launcher will occur at a chamber pressure of 200 bar, which is nearly the chamber pressure of the SSME and RD-O120 engines. The lowest effective net mass for the mixture ratio O_2/H_2 of 7.3:1 is about 51.6 metric tons. The figure contains two families of curves, for the constant Δv of 9300 m/s, and an iteration using the real Δv obtained by the trajectory optimization. The behavior of both families of curves shows no influence from the trajectory calculations, but the effective net mass level is different if the initial Δv_{tot} is not well estimated.

The relatively low optimum chamber pressure of 200 bar for the vehicle with approximately 500 tons of H_2/O_2 propellants is a result of the vehicle choice. Similar but heavier vehicles of a slightly lower technology level consuming 600 tons of H_2/O_2 propellant, as in Manski et al.,[29] have an optimum chamber pressure at 210 bar. Manski and Martin[10] found that a vertical-takeoff, horizontal-landing, single-stage, winged, manned, fully reusable vehicle, which consumes approximately 1300 tons H_2/O_2 propellants for a similar mission, has an optimum chamber pressure above 230 bar. Thus, the optimum chamber pressure is not significantly influenced by large changes in vehicle propellant consumption and weight.

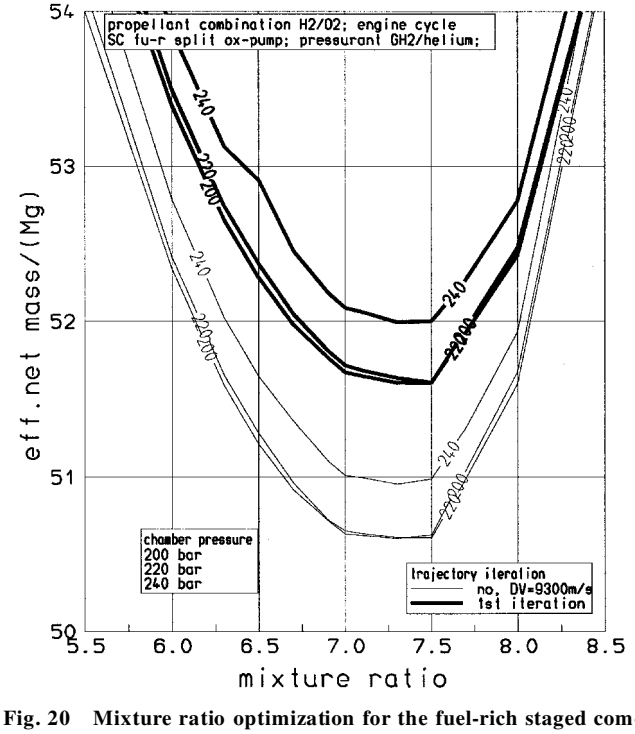

Fig. 20 Mixture ratio optimization for the fuel-rich staged combustion cycle.

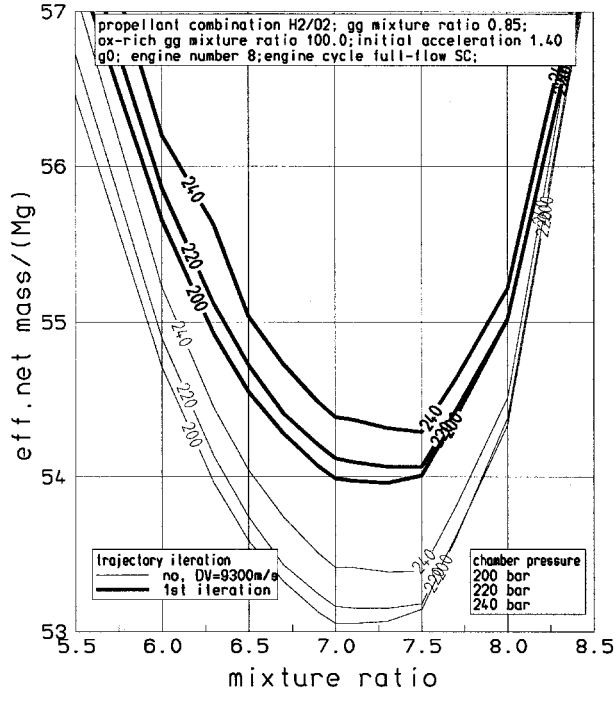

Fig. 21 Mixture ratio optimization for the dual preburning staged combustion cycle.

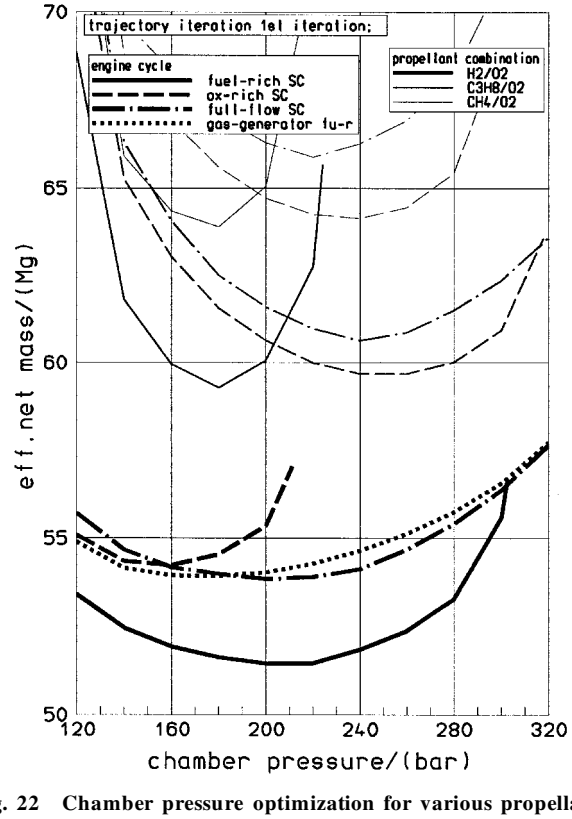

Fig. 22 Chamber pressure optimization for various propellants and cycles at optimum mixture ratio.

Table 3 Summary propulsion system and vehicle data of optimized cycle candidates

	SSTO selected cycles								
Variable	sc fu-ri	Full sc	gg	sc fu-ri	sc ox-ri	dt pro	dt me	dt hy	vm sc
Propellant split pri/total	——	——	——	——	——	0.50	0.50	0.50	0.40
Thrust split pri/tot	——	——	——	——	——	0.29	0.29	0.29	——
Engine number	8	8	8	8	8	4	4	4	8
Propellant combination	H_2/O_2	H_2/O_2	H_2/O_2	C_3H_8/O_2	C_3H_8/O_2	C_3H_8/O_2	CH_4/O_2	H_2/O_2	H_2/O_2
Propellant combi. primary	——	——	——	——	——	H_2/O_2	H_2/O_2	H_2/O_2	H_2/O_2
Propellant combi. secondary	——	——	——	——	——	C_3H_8/O_2	CH_4/O_2	H_2/O_2	H_2/O_2
Pressurant	He/H_2	He/H_2	He/H_2	He/He	He/He	He/H_2	He/H_2	He/H_2	He/H_2
Chamber pressure, bar	200	200	160	200	280	——	——	——	220
Chamber pressure pri, bar	——	——	——	——	——	130	130	130	201
Chamber pressure sec, bar	——	——	——	——	——	220	220	200	220
Mixture ratio	7.3	7.3	6.5	3.3	3.3	——	——	7.0	7.1
Chamber mixture ratio	7.31	7.31	7.18	3.30	3.30	——	——	——	7.50
Mixture ratio pri	——	——	——	——	——	6.5	6.5	6.5	6.5
Mixture ratio sec	——	——	——	——	——	3.3	3.7	7.5	7.5
Nozzle area ratio	59.7	59.7	46.3	66.3	85.8	——	——	——	65.6
Nozzle area ratio primary	——	——	——	——	——	35	35	35	66
Nozzle area ratio secondary	——	——	——	——	——	63	61	54	66
Mode 2 nozzle area ratio	——	——	——	——	——	122	119	118	——
Vacuum specific impulse, Ns/kg	4337	4337	4224	3564	3615	3727	3761	4283	4341
Sea level specific impulse, Ns/kg	3659	3659	3575	2957	3051	3175	3213	3666	3669
Vacuum specific impulse primary, Ns/kg	——	——	——	——	——	4271	4271	4271	4410
Vacuum specific impulse secondary, Ns/kg	——	——	——	——	——	3543	3586	4288	4341
Sea level specific impulse primary, Ns/kg	——	——	——	——	——	3639	3639	3369	3656
Sea level specific impulse secondary, Ns/kg	——	——	——	——	——	3017	3067	3678	3669
Mode 1 sea level *Isp*, Ns/kg	——	——	——	——	——	3175	3213	3666	——
Mode 2 vacuum *Isp*, Ns/kg	——	——	——	——	——	4488	4485	4483	——
Nozzle length 2, m	——	——	——	——	——	——	——	——	0.97
Specific impulse efficiency secondary	0.970	0.970	0.970	0.970	0.970	0.966	0.966	0.966	0.970
Mode1 sea level thrust, kN	——	——	——	——	——	2139	2191	1791	——
Mode2 vacuum thrust, kN	——	——	——	——	——	765	783	640	——
Sea level thrust primary, kN	——	——	——	——	——	620	635	519	6584
Sea level thrust secondary, kN	——	——	——	——	——	1519	1556	1271	7487
Sea level thrust, kN	7866	8115	8567	13,753	13,231	8556	8764	7162	7487
Vacuum thrust, kN	9324	9619	10,122	16,578	15,674	10,044	10,258	8366	8861
Payload, Mg	16.5	16.5	16.5	16.5	16.5	16.5	16.5	16.5	16.5
Payload fairing mass, Mg	2.60	2.60	2.60	2.60	2.60	2.60	2.60	2.60	2.60
Initial mass, Mg	**589.3**	**608.2**	**638.1**	**987.9**	**953.2**	**635.7**	**651.9**	**539.4**	**562.4**
Propellant consum. 1st stage, Mg	521.2	537.7	567.6	911.3	876.7	283.5	290.4	237.3	297.7
Propellant consum. 2nd stage, Mg	——	——	——	——	——	283	290	237	198
Total propellant consumption, Mg	**521.2**	**537.7**	**567.6**	**911.3**	**876.7**	**566.9**	**580.7**	**474.6**	**496.1**
Re-entry mass, Mg	**12.4**	**12.7**	**13.0**	**15.0**	**14.8**	**13.6**	**13.9**	**12.0**	**12.1**
Effective net mass, Mg	**51.6**	**54.0**	**53.9**	**60.1**	**60.0**	**52.3**	**54.7**	**48.3**	**49.8**
All turbo-machinery efficiences	0.75	0.75	0.75	0.75	0.75	0.75	0.75	0.75	0.75
Fu-rich gg char. velocity *c**, m/s	2206	2206	2206	947	——	2206	2206	2206	2206
Ox-rich gg *c**, m/s	——	787	——	——	762	787	787	787	——
Fuel-rich gg temp., K	1006	1006	1006	940	——	1006	1006	1006	1006
Ox-rich gg temp., K	——	997	——	——	985	997	997	997	——
gg-chamber pressure, bar	320	287	160	554	——	241	259	333	373
Ox-rich gg-chamber pressure, bar	——	284	——	——	578.	426.	428.	356.	——
Nozzle exit diameter, m	1.506	1.529	1.555	2.096	1.949	2.173	2.177	1.955	1.461
Engine length, m	2.65	2.68	2.70	3.56	3.37	3.67	3.68	3.32	2.59
Nozzle length, m	2.02	2.05	2.05	2.82	2.66	2.88	2.88	2.58	1.97
Nozzle exit pressure, N/m2	30,000	30,000	32,950	30,000	30,000	35,000	35,000	35,000	30,000
Total velocity capability, m/s	9360	9349	9307	9115	9117	9287	9271	9304	9377
Velocity capability 1st stage, m/s	9360	9349	9307	9115	9117	3386	3434	4160	3271
Velocity capability 2nd stage, m/s	——	——	——	——	——	5901	5837	5143	6106
Structure mass, Mg	**27.0**	**27.5**	**29.5**	**24.4**	**23.7**	**26.8**	**28.3**	**25.8**	**26.5**
Tank mass, Mg	14.4	14.8	16.4	11.1	10.6	12.9	13.9	13.6	14.1
Structural frame, Mg	5.7	5.8	5.9	6.9	6.8	7.0	7.4	5.6	5.7
Pressurization system mass, Mg	.08	.08	.09	.11	.10	.06	.07	.07	.08
Ox tank mass, Mg	4.94	5.06	5.22	7.19	6.84	4.98	5.12	4.59	4.75
Fuel tank mass, Mg	9.48	9.74	11.18	3.90	3.80	7.97	8.76	9.05	9.30
Fuel tank height 1st stage, m	20.27	20.85	24.06	7.85	7.62	16.57	18.01	19.31	19.88
Oxidizer tank height 1st stage, m	10.16	10.43	10.78	14.57	14.08	10.25	10.56	9.37	9.73
H2 tank height, m	20.27	20.85	24.06	7.85	7.62	12.90	13.18	19.31	19.88
HC tank height, m	——	——	——	——	——	3.67	4.83		
Engine mass, Mg	**11.5**	**12.9**	**10.6**	**17.4**	**18.4**	**10.9**	**11.4**	**10.0**	**10.6**
Thrust chamber assembly mass, kg	421	426	464	812	584	903	930	963	395
Control-, turbopump mass, kg	722	889	541	847	1232	1205	1280	1216	650
Thrust chamber mass, kg	217	226	272	449	354	699	721	589	193
Miscellaneous engine, kg	291	301	316	518	490	628	641	523	277
Nozzle mass, kg	204	200	191	362	230	204	209	174	202
GG-mass, kg	70	224	11	77	372	180	184	150	69
Turbo pump mass, kg	400	405	365	431	443	740	786	753	410
Engine valve mass, kg	168	172	165	154	182	254	277	289	171

2. Full-Flow Staged Combustion Cycles

Figure 21 shows similar results for the full-flow staged combustion cycle shown in Fig. 3. The effective vehicle net mass for the best case is 2.3 tons higher or 5% more than the fuel-rich staged combustion cycle. This means more development and production costs for the structure and additional development cost for the more complex engine, in which an oxygen-rich preburner is required.

In earlier investigations[10,29] on the vehicle mentioned in the preceding text, the effective vehicle net mass for the full-flow cycle was also higher for the best chamber pressure and mixture ratio case, and the optimum was found to be a chamber pressure of about 200 bar and a mixture ratio of about 7.5:1. The reason for the increased net mass is that the full-flow cycle requires two preburners, which produces a higher mass for the total engine. For higher chamber pressures, above 290 bar, which is at the limit for the staged combustion cycle with a fuel-rich preburner, the differences in effective net mass become zero or even negative between the two staged combustion cycles, as shown in Fig. 22. The reason for this inverse behavior is the extremely high pressure level required when the simple staged combustion cycles is designed at its thermodynamic limit.

3. Hydrocarbons and Single-Mode Cycles

From the operation cost standpoint, hydrocarbons have many advantages because they are storable for long periods of time. Figure 22 shows a comparison of the performances of hydrocarbons and hydrogen at their optimized mixture ratios using different single-mode cycles. The hydrocarbons require much more effective net mass. The propellant masses consumed are in a range of 1000 tons, but the tank volumes are smaller than for the hydrogen vehicle. For hydrocarbons the oxidizer-rich preburning has the same performance as the fuel-rich preburning, which is the opposite of the hydrogen case. In addition, the optimum chamber pressure for hydrocarbons is higher for oxidizer-rich preburning.

The performance of the gas-generator cycle is shown in Fig. 22 for hydrogen only and for the optimized mixture ratio at 6.5:1. This cycle results in a more effective net mass than the simple-staged combustion cycle. The optimum chamber pressure is low at 160 bar. Table 3 presents a summary of data of the best candidates for propellant combinations and cycles. The mass terms in Table 3 follow the industry standard.[1]

D. Dual-Mode Cycles

Definitions of the terms for the dual-mode cycles are shown in Fig. 23. The mode 1 propellant can include both primary and secondary fuels.

1. Dual-Expander Cycle.

The dual-expander cycle delivers the lowest net mass of all cycles investigated. Figure 24 shows a mass split rate and thrust split rate optimization for the dual-expander cycle using hydrogen for both primary and secondary propellant. These two rates strongly influence the trajectory, so that constant Δv calculations are not applicable. The primary and secondary chamber pressures as well as the primary and secondary mixture ratios given were optimized beforehand. The lowest vehicle effective net mass for this cycle is 4 tons or 8% less than the effective vehicle net mass of the simple-staged combustion cycle, and it is reached at a thrust split rate of 0.3 and a mass split rate of 0.45. The cycle limit can be reached only by thrust split rates at >0.25, because the power balance matching stops at that thrust split rate, chamber pressure, and mixture ratio.

Figure 25 shows a mass split rate and thrust split rate optimization for the dual-expander cycle using hydrogen as the primary and propane as the secondary propellants. The performance is better than that of the single-mode-staged combustion cycle using only propane, but compared to the pure hydrogen dual-expander cycle there are 4 tons more net mass.

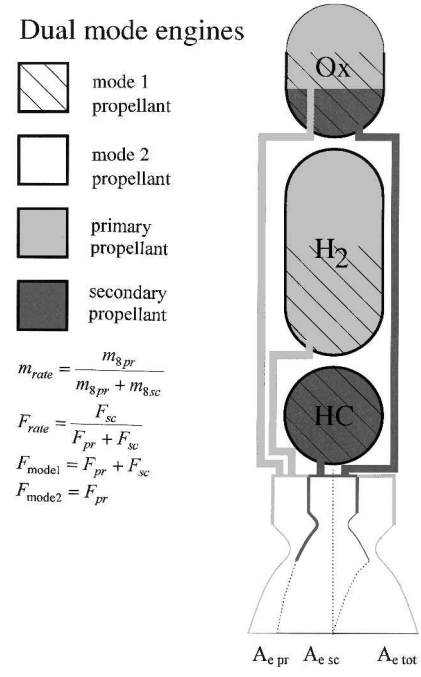

Fig. 23 Dual-mode nomenclature.

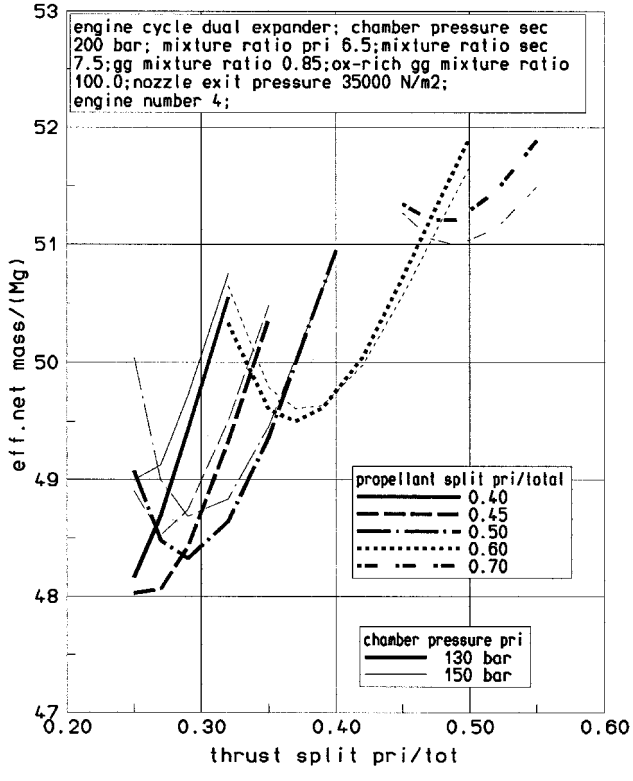

Fig. 24 Dual-expander engine cycle optimization for hydrogen/oxygen.

When using methane in the dual-expander cycle the effective vehicle net mass will again increase. There is no advantage in using hydrocarbons as the second fuel for the dual-expander cycle because of the required higher effective net mass necessary for the vehicle. Of course, this conclusion is strongly dependent on the vehicle chosen. For winged vehicles,[10] using propane as the second fuel in the dual-expander cycle was found to be advantageous. The different result is from a winged vehicle and from different vehicle mass equations, whereas the propulsion mass equations are the same.

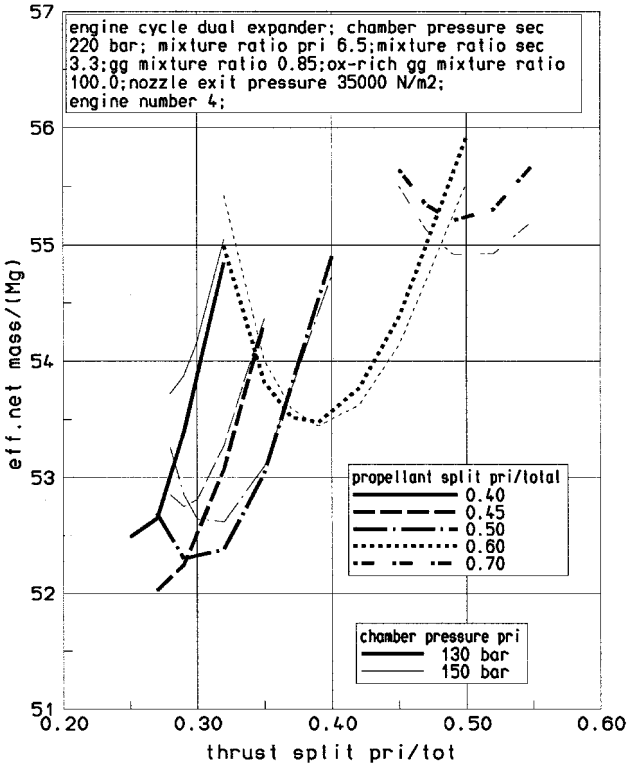

Fig. 25 Dual-expander engine cycle optimization for the tripropellants propane–hydrogen/oxygen.

2. Dual-Fuel Combustion Chamber Cycle

The dual-fuel combustion chamber cycle, often described as the tripropellant cycle (Fig. 17), operates in two different modes. The oxygen is initially burned with kerosene and hydrogen (secondary mode). In the primary mode the relative amount of hydrogen is increased until the burning is completely hydrogen–oxygen. In both modes there is oxidizer-rich preburning (oxygen/kerosene). This cycle is used in the Russian RD-701 design.

The tripropellant cycle is characterized by the following parameters: 1) The propellant split ratio, which gives the amount of propellant mass burned in the primary mode over the total propellant mass burned; 2) the fuel ratio for each mode, which gives the hydrogen mass over the total fuel mass burned in that mode; and 3) the equivalence ratio, which is defined as the stoichiometric mixture ratio over the real mixture ratio.

3. Dual-Thrust Chamber Cycle

Optimizations were reported by Manski and Martin[10] for the dual-thrust chamber cycle applied in reusable, manned, winged SSTO vehicles. The results indicate that this cycle has only slightly higher net masses than the simple-staged combustion cycle and that this cycle is also optimized at a chamber pressure of 200 bar for both chambers and with the same mixture ratio of 7:1. The number of engines was constant for all cycles. If the number of engines for this cycle were reduced by half because of the duplication of thrust chambers, this cycle would show an advantage because of the better specific mass distribution of the turbopump system for each thrust chamber.

4. Dual-Mixture Ratio Cycle

Using the fuel-rich staged combustion cycle as the base for the dual-mixture-ratio vehicles, the dual-mixture-ratio cycle (Figs. 26 and 27) gives a limited advantage of 1% net mass reduction at the optimum set of dual-mixture ratios, first to final, of 7.5–6.5:1, compared with the optimum single mixture ratio at 7.5:1. The relative gain for the single mixture ratio of 7.5:1 was taken from Fig. 26 and not from Fig. 20 because

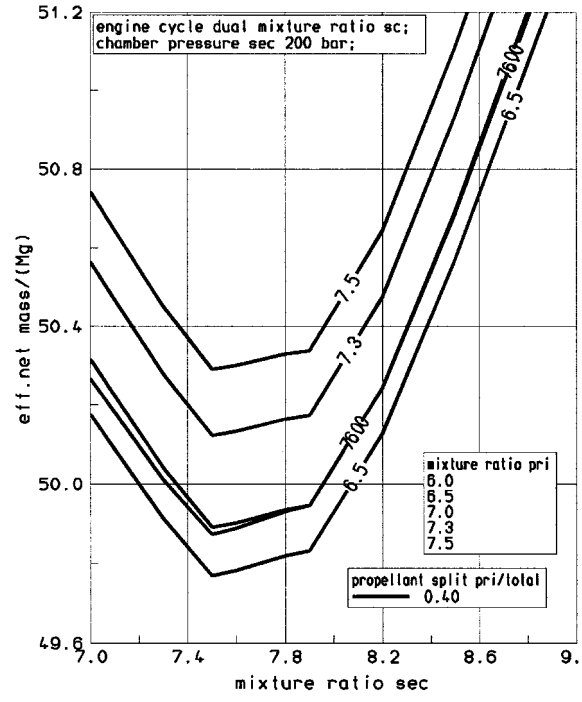

Fig. 26 Dual-mixture ratio cycle optimization.

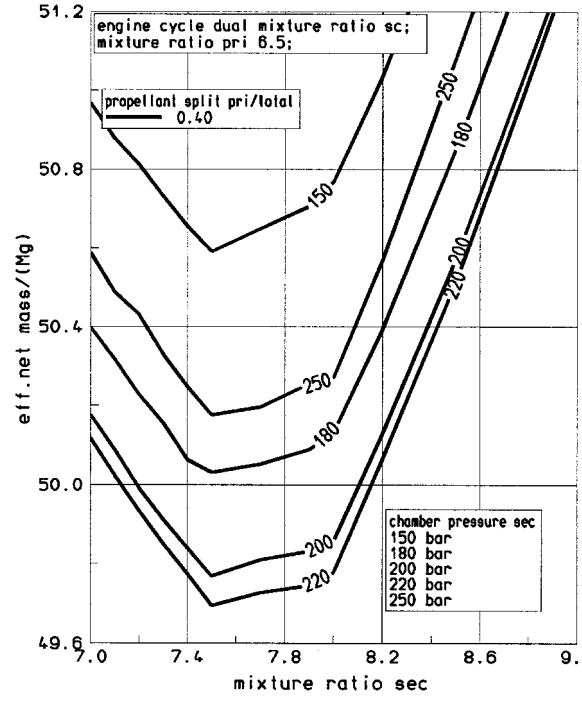

Fig. 27 Dual-mixture ratio cycle optimization vs chamber pressure.

there is a difference caused by vehicle iterations with its primary and secondary propellant loads.

VI. Currently Operational Engine Cycles

Only high-performance engine cycles that produce high chamber pressure (above 200 bar) and are able to deliver 16.5 tons of payload into low Earth orbit by using resuable SSTO vehicles are presented here.

A. Space Shuttle Main Engine

The Space Shuttle Main Engine (SSME) is a reusable, O_2/H_2 staged-combustion engine that operates at a chamber pres-

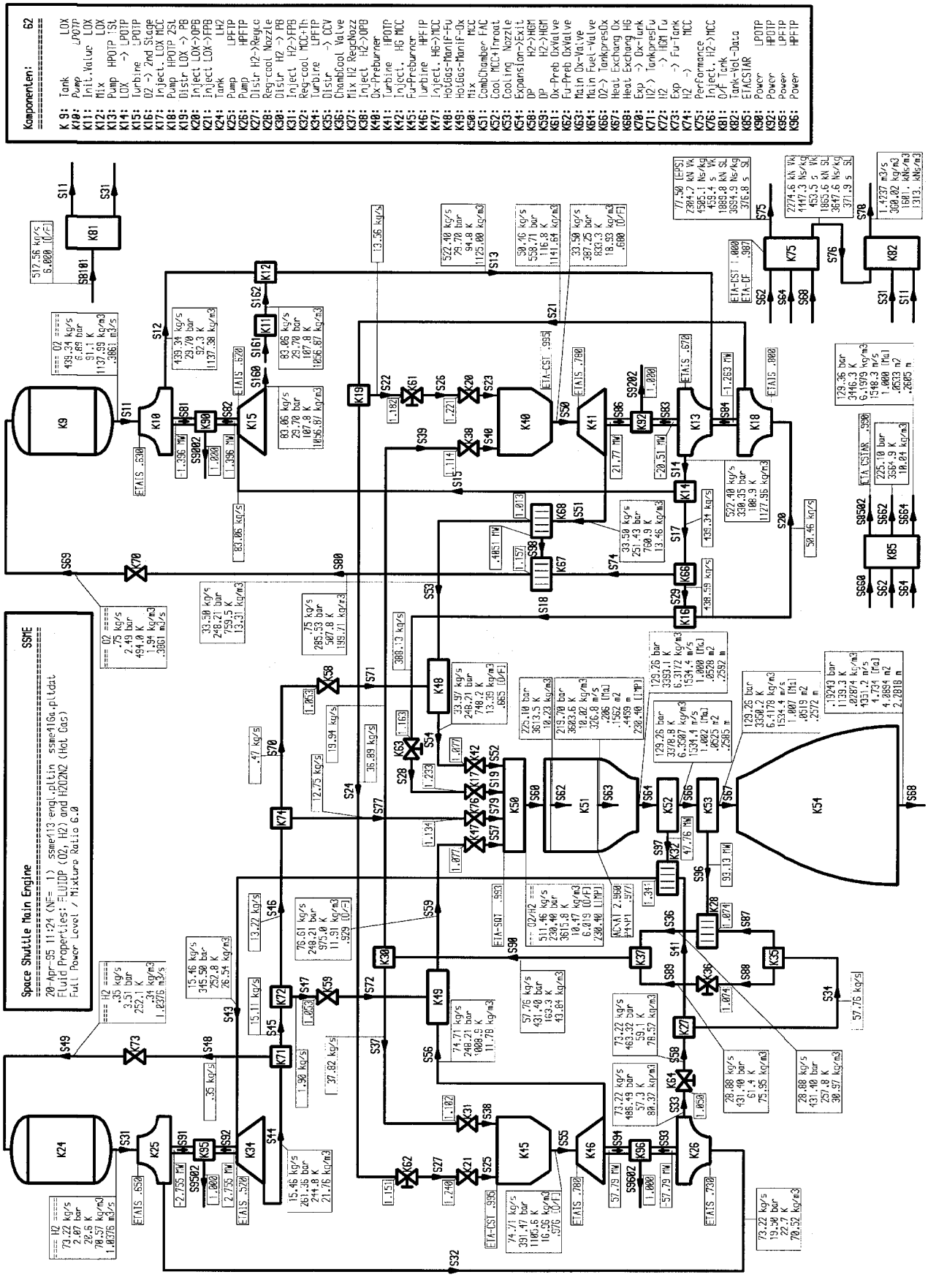

Fig. 28 SSME: modeling and results.

sure of 226 bar. The SSME cycle features dual fuel-rich preburners as shown in Fig. 28 to drive the turbopumps and combustion chamber. The engine has closed-loop control of chamber pressure and mixture ratio and is capable of deep throttling. Since its first flight in 1981, the SSME has gone through several block upgrades to improve operability, reliability, and lifespan, but no change to its engine cycle has been made.

Two low-pressure boost-pumps are employed to raise the propellants from the low tank pressure level to avoid cavitation in the high-speed main pumps. The boost-pumps for hydrogen and oxygen are driven by warm hydrogen and high-pressure liquid oxygen, respectively. There are two regenerative cooling circuits, one for the combustion chamber, throat, and upper part of the nozzle, and the other for the lower part of the nozzle. The modeling in Fig. 28 includes tank pressurization and some smaller hydrogen flows used for cooling gas-generators and turbines. The full power level with a combustion chamber pressure of about 225 bar (total pressure in the finite area combustor) is shown.

Downstream of the low-pressure oxygen turbopump (K10, K15), oxygen from the turbine is mixed into the main flow from the pump. Because turbine K15 follows after mixing element K12 in the sequence of computation, and because every input-dataset has to be known before the calculation, initial values for the turbine output (S160) have to be estimated ($\dot{m}$, p, T in S161) and completed to a full dataset (K11, S162). During iteration, the initial values in S161 are updated to match the turbine output S160.

For the modeling shown in Fig. 28, a total of 62 components, some 200 datasets, and 29 conditions were needed. The combustion chamber was modeled as a finite area combustor, and the influence of nonperfect combustion was treated as a lowering of combustion chamber temperature.

The determination of the optimum nozzle exit pressure for SSTO vehicles in Manski et al.[29] and studies of the SSME for use in an SSTO application indicate that a change of its nozzle expansion from its current 77:1 to 57:1 would be beneficial.[30] The same studies have also considered the conversion of the SSME to a full-flow staged-combustion cycle configuration (Fig. 3).

B. RD-O120

The RD-O120 engine is a flight-qualified liquid oxygen/hydrogen staged combustion engine that has flown twice on the Energia heavy-lift launch vehicle, supplying the main propulsion for the sustainer core stage. Under a typical flight profile it is ignited at sea level and operates about 460 s, producing a nominal vacuum thrust of 2000 kN at 106% of engine thrust, and a vacuum-delivered specific impulse of 4448 Ns/kg.[31] The chamber pressure is 219 bar. Development was begun in 1976, and prior to its inaugural flight in 1987, the RD-O120 completed extensive qualification testing; 163,000 s of testing accumulated on more than 90 engines. It has a demonstrated reliability of 0.992 at 90% confidence.[31] Although it is expendable, the RD-O120 engine was designed to include reusable, durable, and operable features for conducting a cost-effective test program. The reusability and operability of the RD-O120 engine were examined in a recent test program.[32]

A schematic for the RD-O120 engine is shown in Fig. 29, and all of the operating parameters are listed.[23] There are boost pumps for both oxygen and hydrogen to increase suction pressure to the main pumps. The oxygen boost pump has two stages with different rotational speeds, actuated by a hydraulic

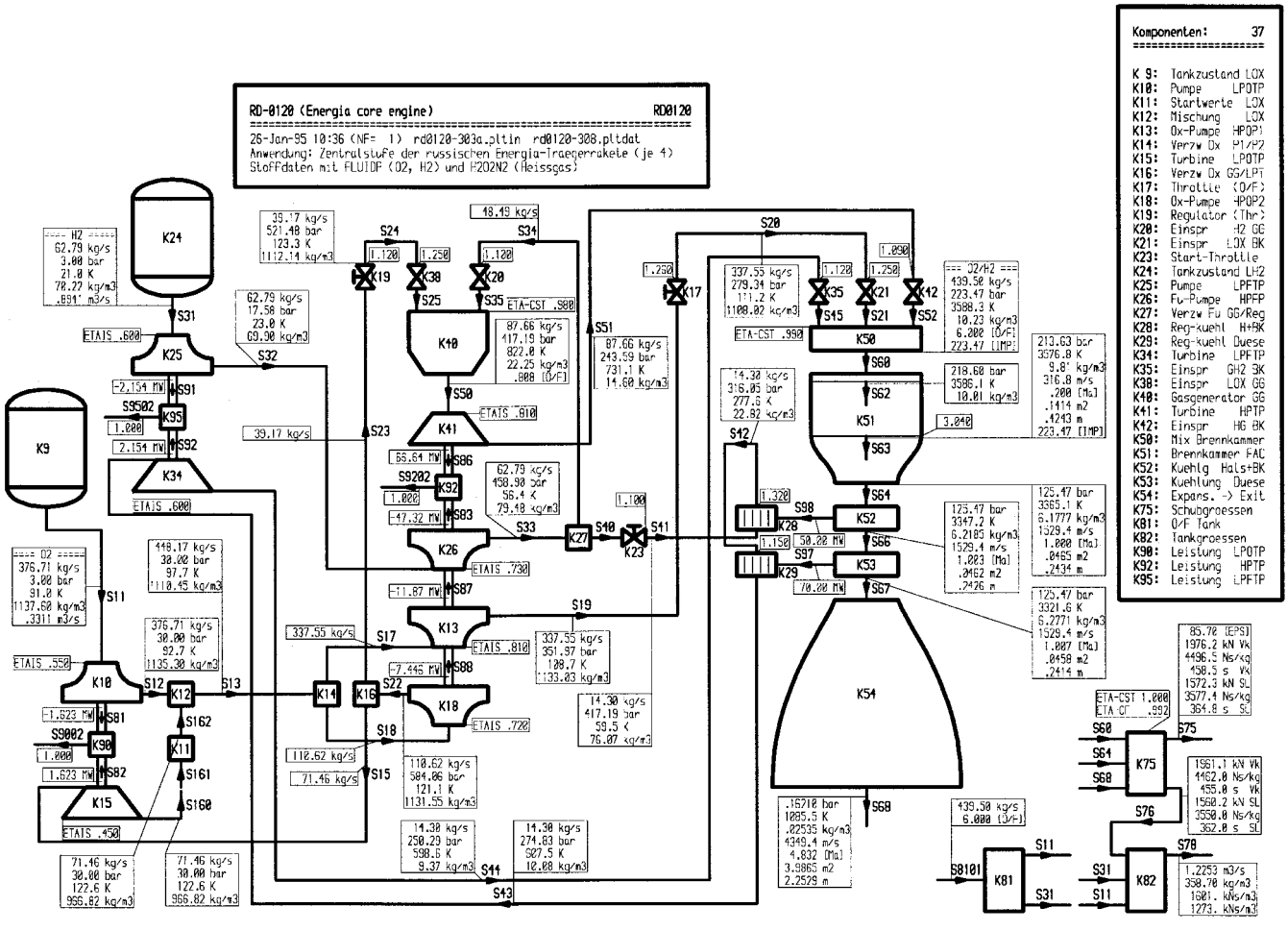

Fig. 29 Modeling and results of the RD-O120 engine.

turbine. The fuel boost pump has one shaft actuated by a gas turbine. The turbopump assembly consists of a three-stage centrifugal hydrogen pump and two-stage axial flow turbine sharing a single rotor and housing, and a centrifugal oxygen pump on a separate subassembly connected to the hydrogen pump shaft with a splined coupling. The oxygen pump has two parallel stages to supply oxygen separately to the preburner and combustion chamber. The turbine is driven with relatively low-temperature (822 K) fuel-rich gas from the preburner. This gas then undergoes secondary combustion in the main combustion chamber.

The combustion chamber and nozzle are cooled regeneratively with 22% of the hydrogen, from the pump third-stage outlet, through milled coolant channels. This hydrogen is then used to drive the hydrogen boost pump turbine before being injected into the main chamber as injector face coolant.

The power and mixture ratio regulation system includes two electromechanically actuated valves. One controls oxidizer flow rate to the preburner for engine thrust level control and to ensure a controlled engine start, and the other controls oxidizer flow rate to the main combustion chamber for engine mixture ratio control.

C. RD-170

The RD-170 engine[33] is a flight-qualified liquid oxygen/kerosene staged combustion engine for the Russian Zenit medium lift launcher and the Energia heavy-lift launch vehicle, supplying boost stage propulsion.

A schematic for the RD-170 engine is shown in Fig. 30 and operating parameters are listed.[23] The RD-170 has four combustion chambers fed by a single turbopump driven by gas from an oxidizer-rich preburner. There are boost pumps for oxygen and kerosene. The oxygen boost pump is driven by oxidizer-rich gas, whereas the fuel boost pump is driven by high-pressure kerosene. The turbopump assembly consists of centrifugal oxygen and kerosene pumps, a high-pressure kick-stage pump for a supply of kerosene to the preburners, and an axial flow turbine. The turbine is driven with a relatively low temperature (790 K) oxidizer-rich gas from the preburner. This gas then undergoes secondary combustion in the main combustion chamber.

The combustion chamber and nozzle are cooled regeneratively with the remainder of the kerosene that is not supplied to the preburner. The warmed kerosene is then supplied to the main injector to react with the warm oxidizer-rich gas from the turbine exhaust. The nozzle and combustion chamber use milled coolant channels.

VII. Future Engine Cycles

A. RS-2200

Designed from the ground up to reduce costs in every phase of its operation, the VentureStar™ reusable SSTO will employ

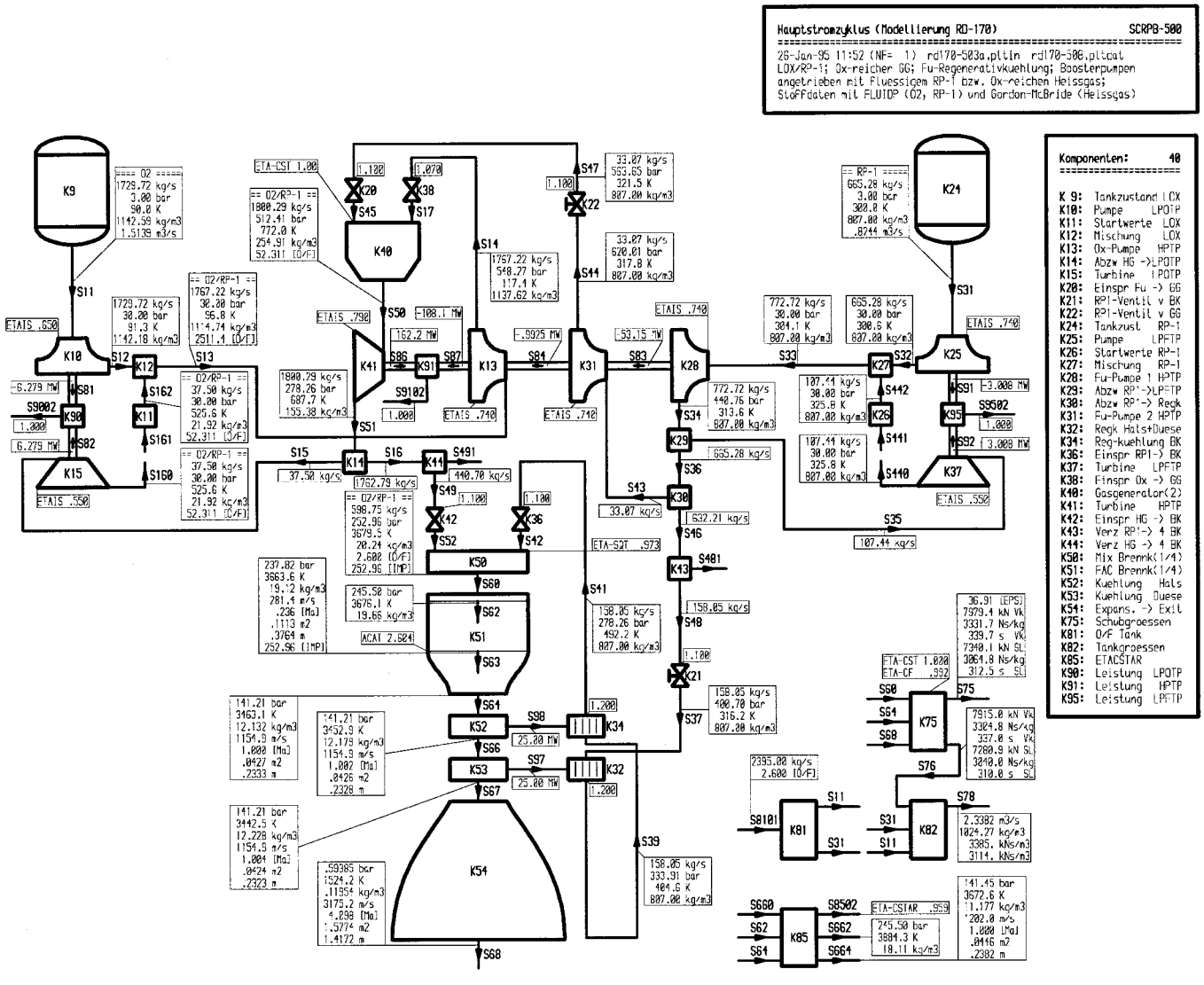

Fig. 30 Modeling and results of the RD-170 engine.

a linear aerospike engine for maximum performance with minimum weight. This engine, designated the RS-2200, is a fuel-rich gas-generator cycle similar to the one shown in Fig. 5, and it is operating at a nominal 155-bar chamber pressure. To minimize the open-cycle performance decrement, the RS-2200 operates with high gas-generator temperature and uses the turbine exhaust to act on the aerospike base to produce additional thrust. Early design studies showed that the improved engine thrust-to-weight of the gas-generator cycle as compared to closed-cycle alternatives more than offset the few seconds of specific impulse decrease. The thrust-to-weight advantage of the gas-generator lies primarily in lower ducting weight (liquid lines rather than hot gas lines) and in simpler valving for engine control.

The VentureStar will be preceded by the X-33 test flight vehicle. Among the technologies to be demonstrated on the X-33 is a linear aerospike engine, traceable to the RS-2200, designated the XRS-2200. The XRS-2200 is a 59-bar, fuel-rich, gas-generator engine that utilizes powerhead components from the Apollo program's J-2 engine.

B. RD-701

Figure 31 shows the tripropellant engine based on an oxidizer-rich staged combustion preburner cycle that uses a combination of liquid oxygen, kerosene, and liquid hydrogen as propellants.[23] The basis for this tripropellant engine cycle is the RD-170 engine. A multiple nozzle version, similar to the RD-170, is called the RD-701, whereas a single nozzle version, used for U.S. SSTO packaging and thrust requirements, is called the RD-704.

The two high-pressure turbopumps are driven by oxidizer-rich hot gas produced in two separate gas-generators. Hydrogen is employed for regenerative cooling of the combustion chamber and nozzle. The oxygen boost-pump is driven by oxidizer-rich/kerosene hot gas, the kerosene boost-pump is driven by compressed kerosene, and warm hydrogen is used to drive the hydrogen boost-pump as in the SSME.

An attempt has been made to match the main characteristics of the RD-701 engine in the tripropellant mode. The RD-701 is briefly described by Tkachenko et al.,[34] but no detailed data or engine scheme are available. The analysis shows that the very high chamber pressure of 294 bar (S61) can only be realized with very good turbopump efficiencies, small pressure losses, and rather high preburner temperatures. Even with the optimistic assumptions made for the analysis shown in Fig. 31, the maximum pressure in the system (939 bar in S26 after the kerosene-kickpump) and the preburner pressure (816 bar in S50 and S52) appear to be very high. The methods used to obtain high combustion efficiency with this scheme were addressed by Lozino-Lozinskaya et al.[35]

Another version of a tripropellant engine has been proposed based on a fuel-rich staged combustion preburner cycle, using the RD-O120 engine as the basis for the cycle.[36] This tripropellant engine concept is a dual-mode engine in which the first operating mode, for liftoff on the ground, is tripropellant

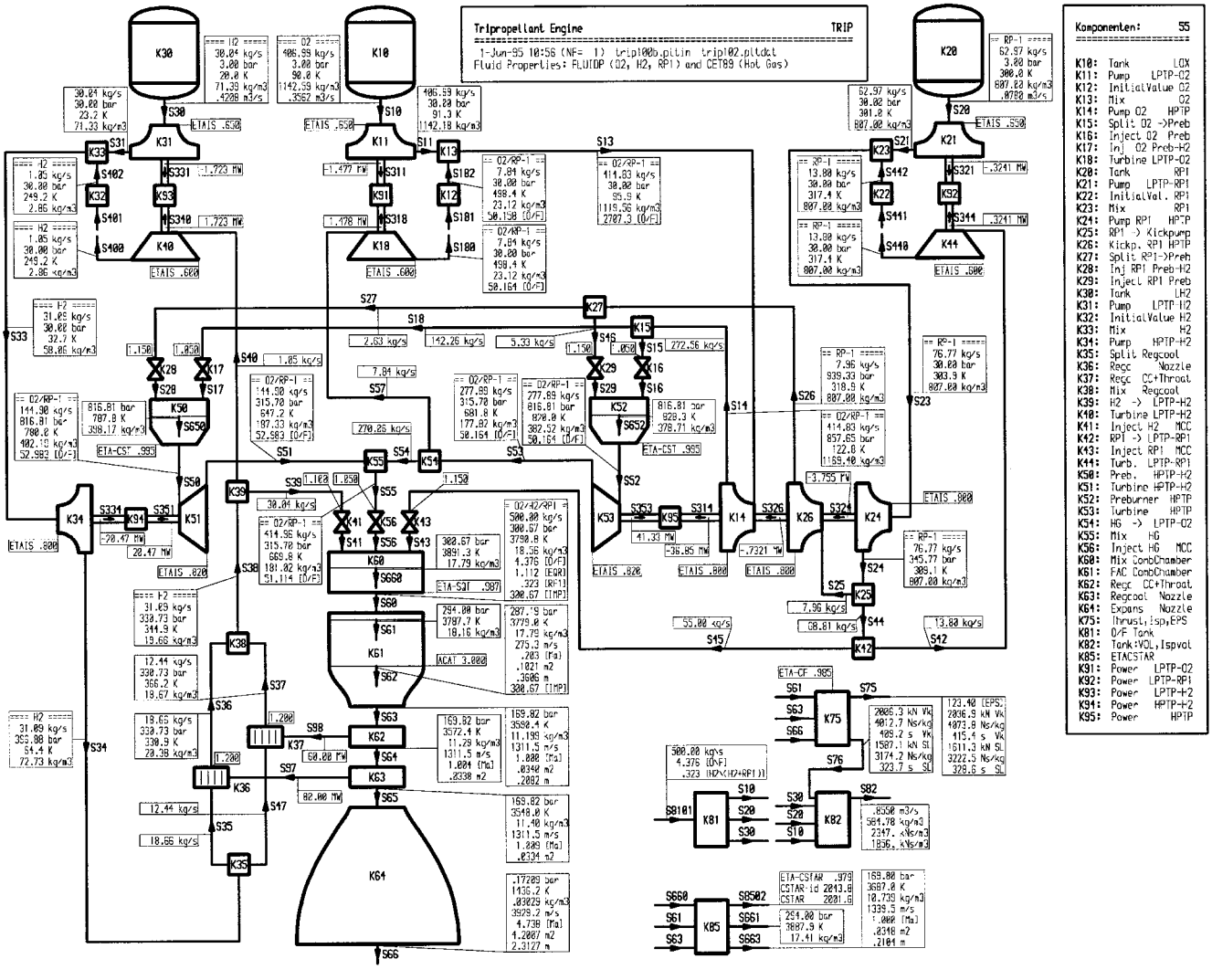

Fig. 31 Modeling and results of a tripropellant engine.

(hydrocarbon + liquid hydrogen + liquid oxygen), and the second operating mode, for sustained performance at altitude, is bipropellant (liquid hydrogen + liquid oxygen). The concept and the cycle scheme are briefly described Gontcharov et al.[36]

C. Additional Engines

Recent studies by Goracke[37–39] have shown that the full-flow, staged-combustion, O_2/H_2 bell nozzle engine may have advantages for use in SSTO missions. This analysis presents a contrast to that made in Sec. V.C.2, which is not positive toward this engine cycle. In support of the X-33 and Reusable Launch Vehicle programs, an engine system designated the RS-2100 was developed,[40] using the full-flow cycle as shown in Fig. 3. The RS-2100 is a major evolution of the SSME in which improved performance, e.g., 40% thrust-to-weight, and operational characteristics, e.g., 50% fewer critical failure modes, have been added at the same chamber pressure and thrust operating point as the SSME. The cycle selection permits operation at low turbine temperatures, which eliminates the need for coatings and for actively cooled ducting and permits robust design within the plateau region of aerospace material strengths. Because the RS-2100 cycle uses turbine-drive gases identical with the pumped liquid, the turbomachinery is also greatly simplified with the elimination of elaborate fluid isolation seals.

VIII. Summary and Conclusions

The technology levels needed for single-mode cycle engines for future SSTO vehicles have already been reached by the SSME and RD-O120 engines. A staged combustion cycle with a single fuel-rich preburner producing a chamber pressure of only 200 bar will be sufficient to power an SSTO vehicle to deliver 16.5 tons into low Earth orbit and return back to Earth. The full-flow staged combustion cycle results in heavier vehicle net masses. The dual-expander cycle, which consumes only H_2/O_2 in the two modes, is a higher-performing cycle that can result in 10% lower vehicle net masses. The dual-mixture ratio cycle offers only a small advantage.

References

[1]Koelle, H. H. (ed.), *Handbook of Astronautical Engineering*, McGraw–Hill, New York, 1961.

[2]Manski, D., "Analysis and Optimization of Small Space Shuttle Propulsion Platforms," European Space Agency, ESA-TT-901, English version of DFVLR-FB-84-28, Paris, France, June 1985.

[3]Manski, D., and Rosen, S. G., "A Novel Feed System for the Space Shuttle Payload Propulsion Platform," AIAA Paper 88-2279, July 1988.

[4]Manski, D., and Martin, J. A., "Optimization of the Propulsion Cycles for Advanced Shuttles. Part 2: Performance Model Methodology," AIAA Paper 90-2436, July 1990.

[5]Kozlov, A. A., Hinckel, J. N., and Comiran, A., "Investigation of a Nozzle Tap-Off Liquid Rocket Engine Scheme," AIAA Paper 96-3118, July 1996.

[6]Nakatsuji, H., and Manski, D., "Feasibility Study of Improved Expander-Bleed Cycle and Expander Cycle Engines for SSTO," *Proceedings of the 20th International Symposium on Space Technology and Science* (Gifu, Japan), 1996. (ISTS-96-a-2-9).

[7]Nakatsuji, H., "Feasibility Study of Improved Expander-Bleed Cycle and Expander Cycle Engines for SSTO Vehicles," DLR-IB 645-96/24, DLR, Lampoldshausen, Germany, Jan. 1996.

[8]Tanatsugu, N., Naruo, Y., and Suzuki, K., "Preliminary Experiment on Lox/LH_2 High Pressure Expander Cycle Engine," *Acta Astronautica*, Vol. 15, No. 6/7, 1987, pp. 347–352.

[9]Goracke, B., Levack, D., and Nixon, R., "Advanced, Low-Cost O_2/H_2 Engines for the SSTO Application," AIAA Paper 94-3317, June 1994.

[10]Manski, D., and Martin, J. A., "Evaluation of Innovative Rocket Engines for Single-Stage Earth-to-Orbit Vehicles," *Journal of Propulsion and Power*, Vol. 7, No. 6, 1991, pp. 929–937.

[11]Beichel, R., "The Dual-Expander Rocket Engine—Key to Economical Space Transportation," *Astronautics and Aeronautics*, Nov. 1977.

[12]Taniguchi, H., and Manski, D., "Performance of Advanced Engine Cycles in Future Launcher," 38th International Astronautical Congress, IAF 87-288, Brighton, England, UK, Oct 1987.

[13]Hagemann, G., Immich, H., Nguyen, T. V., and Dumnov, G. E., "Advanced Rocket Nozzles," *Journal of Propulsion and Power*, Vol. 14, No. 5, 1998, pp. 620–634.

[14]Manski, D., Taniguchi, H., and Saßnick, H. D., "Comparative Analysis of the Vulcan and the LE-7 Engines Applied in Ariane 5 and H-II Launchers," 16th ISTS, Sapporo, Japan, May 1988.

[15]Manski, D., and Fina A., "Advanced Rocket Propulsion Systems for Reusable Ballistic Single-Stage-to-Orbit Vehicles BETA & Delta-Clipper," AIAA Paper 94-3316, June 1994.

[16]Manski, D., and Martin, J. A., "Optimization of the Propulsion Cycles for Advanced Shuttles. Part 1: Propulsion Mass Model Methodology," AIAA Paper 89-2279, June 1989.

[17]Manski, D., "Effects of Engine Cycle Type on Payload Delivery of the Future European Launchers," International Astronautical Federation, 36th International Astronautical Congress, IAF 85-127, Stockholm, Sweden, Sept. 1985; *Zeitschrift für Flugwissenschaft*, Vol. 10, No. 2, 1986, pp. 51–61.

[18]Manski, D., "ST-TRANSYS, Cycles Considered, Subroutine Classification, Application Programming Interface," DLR IB 645-96/02, Lampoldshausen, Germany, 1996.

[19]Rommel, T., Hagemann, G., Schley, C.-A., Manski, D., and Krülle, G., "Plug Nozzle Flowfield Calculations for SSTO Applications," AIAA Paper 95-2784, June 1995.

[20]Hagemann, G., Manski, D., and Krülle, G., "Dual Expander Engine Flowfield Simulations," AIAA Paper 95-3135, June 1995.

[21]Manski, D., and Hagemann, G., "Influence of Rocket Design Parameters on Engine Nozzle Efficiencies," AIAA Paper 94-2756, June 1994.

[22]Manski, D., "Comparison of Kinetic, Equilibrium and Frozen Rocket Expansion Obtained at Different Propulsive Parameters for Launcher and Spacecraft Engines," DLR-Mitt. 91-02, DLR, Cologne, Germany, Feb. 1991.

[23]Goertz C., "A Modular Method for the Analysis of Liquid Rocket Engine Cycles," AIAA Paper 95-2966, July 1995.

[24]Saßnick, H. D., "Numerical Simulation of Non-Stationary Condition in Cryogenic Rocket Engines," ISRN DLR-FB-96-17, Cologne, Germany, 1996 (in German).

[25]Saßnick, H. D., "Numerical Simulation of Transients in Feed Systems for Cryogenic Rocket Engines," AIAA Paper 95-2967, July 1995.

[26]Koelle, D. E., and Kleinau W., "The Single-Stage Reusable Ballistic Launcher Concept for Economic Cargo Transportation," International Astronautical Federation, IAF-86-122, Innsbruck, Austria, Oct. 1986.

[27]Weegar R. K., "Engine/Vehicle Integration for Vertical Takeoff and Landing SSTO Vehicles," International Astronautical Federation, IAF-92-065, Washington, DC, Oct. 1992.

[28]Bauer, G. L., Cornick, D. E., and Stevenson, R., "Capabilities and Applications of the Program to Optimize Simulated Trajectories (POST)," NASA-CR-2770, 1977.

[29]Manski, D., Hagemann, G., and Saßnick, H. D., "Optimization of Dual Expander Rocket Engines in Single-Stage-to-Orbit Vehicles," International Astronautical Federation, 47th International Astronautical Congress, IAF-96-S.2.05, Beijing, PRC, Oct. 1996.

[30]Aldrich, A., "Access to Space Study," NASA, Jan. 1994.

[31]Rachuk, V. S., Goncharov, N. S., Martynyenko, Y. A., Barinshtein, B. M., and Sciorelli, F. A., "Design, Development, and History of the Oxygen/Hydrogen Engine RD-O120," AIAA Paper 95-2540, July 1995.

[32]Rachuk, V. S., Shostak, A. V., Dmitrenko, A. I., Goncharov, G. I., Hernandez, R., Starke, R. G., and Hulka, J., "Benchmark Testing of an Enhanced Operability LO2/LH2 RD-O120 Engine," AIAA Paper 96-2609, July 1996.

[33]Katorgin, B. I., Chelkis, F. J., and Limerick, C. D., "The RD-170, A Different Approach to Launch Vehicle Propulsion," AIAA Paper 93-2415, June 1993.

[34]Tkachenko, J. N., and Limerick, C. D., "Powerful Liquid Rocket Engine (LRE) Created by NPO Energomash for Up to Date Space Rockets," AIAA Paper 93-1957, June 1993.

[35]Lozino-Lozinskaya, I. G., Chelkis, F. J., and Tanner, L. G., "The Current Status of Tripropellant Combustion Technology," 2nd International Symposium of Liquid Rocket Propulsion, ONERA, Châtillon, France, June 1995, p. 24-1.

[36]Gontcharov, N. S., Orlov, V. A., Rachuk, V. S., Rudis, M. A.,

Shostak, A. V., McIlwain, M. C., Starke, R. G., and Hulka, J., "Tripropellant Liquid Rocket Engine Technology Using a Fuel-Rich Closed Power Cycle," *Proceedings of the 2nd International Symposium of Liquid Rocket Propulsion*, (Châtillon, France), 1995.

[37]Goracke, B., Levack, D., amd Nixon, R., "Margin Considerations in SSTO O_2/H_2 Engines," AIAA Paper 94-4676, Sept. 1994.

[38]Goracke, B., Levack, D., and Johnson, G., "Tripropellant Engine Drive Cycle Considerations for the SSTO Application," AIAA Paper 95-2950, July 1995.

[39]Goracke, B., Levack, D., and Johnson G., "Tripropellant Engine Option Comparison for SSTO," AIAA Paper 95-3609, Sept. 1995.

[40]Davis, J., and Campbell, R., "Advantages of a Full-Flow Combustion Cycle Engine System," AIAA Paper 97-3318, July 1997.

[41]Martin, J. A., and Manski, D., "Variable-Mixture-Ratio and Other Rocket Engines for Advanced Shuttles," *Journal of Propulsion and Power*, Vol. 7, No. 4, 1991, pp. 549–555.